Materials Science in Semiconductor Processing 141 (2022) 106400

Contents lists available at ScienceDirect

Materials Science in Semiconductor Processing

journal homepage: www.elsevier.com/locate/mssp

Full length article

Strain effect on the intraband absorption coefficient for spherical CdSe/CdS/ZnSe core–shell–shell quantum dots

K.A. Rodríguez-Magdaleno [a,*], R. Pérez-Álvarez [b,c], F. Ungan [d], J.C. Martínez-Orozco [a]

[a] Unidad Académica de Física, Universidad Autónoma de Zacatecas, Calzada Solidaridad esquina con Paseo La Bufa S/N, C.P. 98060, Zac., Zacatecas, Mexico
[b] Centro de Investigación en Ciencias, Instituto de Investigación en Ciencias Básicas y Aplicadas, Universidad Autónoma del Estado de Morelos, Av. Universidad 1001, CP 62209, Cuernavaca, Morelos, Mexico
[c] Unidad Académica de Ciencia y Tecnología de la Luz y la Materia, Universidad Autónoma de Zacatecas, Carretera Zacatecas-Guadalajara Km. 6, Ejido La Escondida, 98160 Zacatecas, Zac., Mexico
[d] Department of Physics, Faculty of Science, Sivas Cumhuriyet University, 5814, Sivas, Turkey

ARTICLE INFO

Keywords:
Strain effect
Absorption coefficient
Spherical quantum dot
Intraband transitions

ABSTRACT

In this work, we theoretically calculated the intraband absorption coefficient (IAC) between the $1s$ and $1p$ conduction band states for a spherical core/shell/shell quantum dot (CSS-QD) as function of inner and outer shells' sizes with and without the presence of strain effect. The electronic structure for the system is computed in the effective mass approximation framework and the strain effect is considered on the continuum elasticity model. We found out that as we compared the strained and the unstrained system, the former causes that the IAC undergoes a small redshift. A similar behavior occurs as the inner and outer shell size increase. The results show that the strain effect is an important factor that will be considered in these nanostructure type. The incorporation of inner and outer shells allowed us to extend some fractions of eV into the absorption spectrum that could be interesting as a mechanism to control the IAC device design.

1. Introduction

The semiconductor quantum dots (QDs) have attracted much attention due to the several device applications [1–4] particularly the related ones with the optical properties. Molecular Beam Epitaxy (MBE), Metal-Organic Chemical Vapor Deposition (MOCVD), and in general the synthesis by chemical methods allow the experimentalist to grow semiconductor QDs with several geometries. In this regard, the core–shell quantum dots (CS-QDs) system is experimentally feasible and basically consist of a spherical QD of some semiconductor material (which in this case represents the core) covered by another semiconductor material, commonly known as a shell. Recently, Young-Shin Park et al. [5] published a report that assets that the optical properties can be easily controlled by the quantum confinement and probably, among several possible applications, the colloidal QD lasers reflects the accumulated knowledge on the QDs, the CS-QDs also included. Typically, the CS-QDs are compound by II–VI, III–V, and IV–VI semiconductor materials, and the physical properties depends on the band-gaps and the band offsets as well as on the lattice mismatch because the heterostructure could be type-I or -II and the strain effect could also of paramount importance on the optoelectronic properties.

Several authors have theoretically studied III–V CS-QDs, they mainly reported that the optical properties strongly depends on the QD size and on the shape of the confinement potential, as well as on the incorporation of donor impurities, the presence of electric and magnetic fields and by hydrostatic pressure effects [6–21]. On the other hand, II–VI core–shell and core–shell–shell QDs composed by semiconductors as CdSe/CdS, CdSe/HgS, CdSe/PbS, ZnSe/ZnSe, ZnS/CdS, CdSe/CdS/ZnS, CdSe/ZnSe/ZnS and CdTe/CdS/ZnS have been also reported by experimental researchers [22–24]. When semiconductors with different lattice parameters are in contact, a lattice mismatch in the interface is present and consequently, an elastic strain effect is part of the system. The strain has a vital role on the physical properties for the semiconductor heterostructure. A.M. Smith et al. [25] experimentally found that the strain effect clearly modifies the electronic band structure, and consequently it affects the optical properties. Theoretically, the core–shell ZnTe/ZnSe, and CdTe/ZnSe QDs strain is reported by T.O. Cheche et al. [26,27], they considered the shell's size to change the electronic properties. Strain studies on the inter-band absorption coefficient and photo-excited carrier localization are also calculated in CdSe/CdS/ZnS, ZnTe/ZnSe/ZnS CSS-QDs by T.E. Pahomi and coworkers [28]. Theoretical comparison of the electron and hole states, and the emission spectrum of InP/ZnSe/ZnS and CdSe/ZnSe/ZnS heterostructures were investigated [29]. Recently, the size dependent strain effect in the

* Corresponding author.
E-mail address: karelyrod@uaz.edu.mx (K.A. Rodríguez-Magdaleno).

https://doi.org/10.1016/j.mssp.2021.106400
Received 9 June 2021; Received in revised form 23 November 2021; Accepted 8 December 2021
Available online 5 January 2022
1369-8001/© 2021 Elsevier Ltd. All rights reserved.

conversion efficiencies (CE) for a CS-QD is studied in [30,31], the results show that the strain effect has a very important influence on the CE. Model solid theory [32] and continuum elasticity model (CM) [28] have been used to determinate the strain effects.

Related with the strain effect, there are theoretical works where different approaches have been used to calculate the electronic structure [33–35]. Optical properties are reported by different authors also. For instance, R. Kostić and D. Stojanović [36] calculated the oscillator strengths and report the intersubband optical absorption coefficient considering third-order nonlinear contributions in a CdSe/ZnS/CdSe/SiO_2 spherical QD. The optical absorption coefficient (OAC) is obtained in CdSe/CdS/CdSe/CdS, CdSe/$Pb_{1-x}Cd_xSe$/CdSe, CdSe/ZnTe, CdSe/ZnS CS-QDs in Refs. [37–40]. In these works, we can see that the OAC strongly depends on the size and composition semiconductor materials of CS-QDs. An important study of the absorption coefficient of CdSe/ZnS and ZnS/CdSe CS-QD in the case of luminescent solar concentrators (LSCs) is conducted by Bahareh et al. [41], their results show that the CS-QDs can absorb higher energy photons in solar spectrum in comparison with the inverted CS-QDs. In the previous works, interesting results are shown for CS-QDs systems, however, it is also possible to have another shell, so we considered the strain effect in a CdSe/CdS/ZnSe CSS-QD as function of the shells' sizes. The importance of this contribution is that we considered the strain effect, by working within the effective mass theory, for the case of CdSe/CdS/ZnSe spherical quantum dot following the lines of T.E. Pahomi [42]; additionally, it is relevant to say that core/shell and core/shell/shell spherical heterostructures are experimentally feasible. The aim of this study is to exhibit how the intraband absorption coefficient could be tuned in different regions of the absorbed photon energy. The study is carried out within the effective mass approximation, considering parabolic bands, and the strain effect is considered by the model solid theory and continuum elasticity model.

The organization of the paper is the following: Section 2 describes the studied system and the theoretical used model to calculate the electronic and intraband absorption coefficient. Section 3 shows the results of the electronic states, energies and intraband absorption coefficient as a function of shell's sizes. The conclusions are finally presented in Section 4.

2. Theoretical framework

In this work, we theoretically studied the intraband absorption coefficient for a spherical CSS-QD composed by a CdSe core, covered with inner and outer shells of CdS and ZnSe semiconductor materials, respectively. The main transition is considered between the $1s$ and $1p$ electron states. A schematic representation of the CSS-QD is presented in Fig. 1. Here r_{CdSe}, w_{CdS}, and w_{ZnSe} are the core radius and the inner and outer shells widths.

The electronic structure is calculated by a finite difference method within the framework of the effective mass approximation. The confined energies and the wave functions for the electronic states are obtained by the BenDaniel–Duke equation [43]

$$\left[-\frac{\hbar^2}{2}\nabla\cdot\left(\frac{1}{m^*}\nabla\right)+V(\vec{r})\right]\psi(\vec{r})=E\psi(\vec{r}), \tag{1}$$

where $\hbar$ is the reduced Planck constant, m^* is the isotropic electron effective mass in each region, $V(\vec{r})$ is the confinement potential, E are the energy level spectrum and $\psi(\vec{r})$ stands for the envelope function.

For the CSS-QD, we considered a spherical symmetry, such that we can separate the envelope function in angular and radial components:

$$\psi(r,\theta,\phi)=R_{n\ell}Y_\ell^m(\theta,\phi), \tag{2}$$

being $R_{n\ell}$ the radial wave function and $Y_\ell^m(\theta,\phi)$ the well known spherical harmonics. The radial wave functions are calculated by

$$\left[-\frac{\hbar}{2}\frac{d}{dr}\left(\frac{1}{m^*}\frac{d}{dr}\right)+\frac{\ell(\ell+1)\hbar^2}{2m^*r^2}+V(r)\right]U_{n\ell}(r)=EU_{n\ell}(r), \tag{3}$$

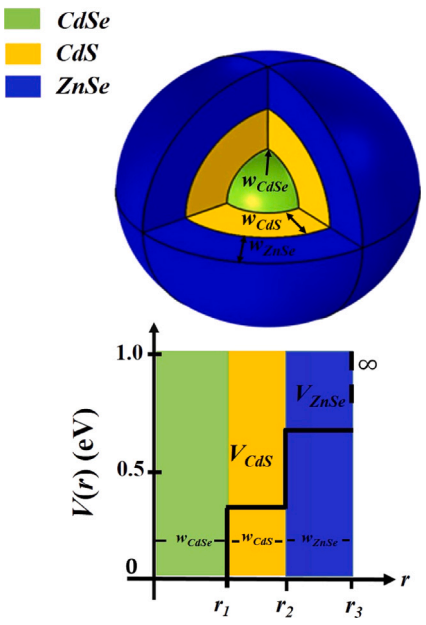

Fig. 1. CdSe/CdS/ZnSe CSS-QD schematic representation and the correspondingly confinement potential profile. The core radius and shells widths are represented as r_{CdSe}, w_{CdS} (r_2-r_1) and w_{ZnSe} (r_3-r_2).

where $U_{n\ell}(r)=rR_{n\ell}(r)$, and the subscripts n and ℓ label the principal and the angular quantum number, respectively. The confinement potential (Fig. 1) is given by:

$$V(r)=\begin{cases}0, & 0\le r\le r_1\\ V_{CdS} & r_1<r\le r_2\\ V_{ZnSe}, & r_2<r\le r_3\\ \infty & r>r_3,\end{cases} \tag{4}$$

with $V_{CdS}=E_c^{CdS}-E_c^{CdSe}$ and $V_{ZnSe}=E_c^{ZnSe}-E_c^{CdS}$ and, according with the model-solid theory, the value of the strained conduction band edge is

$$E_c=E_c^0+a_c\frac{\Delta\Omega}{\Omega} \tag{5}$$

where $E_c^0=E_g^0+E_v^0$ is the unstrained band edge values, a_c stands for the hydrostatic deformation potentials, $\Delta\Omega/\Omega$ represents the fractional volume change, also denoted as ε_{hyd}.

According to the expressions obtained by T.E. Pahomi [42], the ε_{hyd} within the continuum elasticity approach, for the radial displacement, is described by

$$\varepsilon_{hyd}^{CdSe}=2\frac{1-2\nu_{CdSe}}{1-\nu_{CdSe}}\left[\varepsilon_1\left(1-\frac{r_1^3}{r_3^3}\right)+\varepsilon_2\left(1-\frac{r_2^3}{r_3^3}\right)\right], \tag{6}$$

$$\varepsilon_{hyd}^{CdS}=2\frac{1-2\nu_{CdS}}{1-\nu_{CdS}}\left[-\varepsilon_1\frac{r_1^3}{r_3^3}+\varepsilon_2\left(1-\frac{r_2^3}{r_3^3}\right)\right], \tag{7}$$

$$\varepsilon_{hyd}^{ZnSe}=-2\frac{1-2\nu_{ZnSe}}{1-\nu_{ZnSe}}\left(\varepsilon_1\frac{r_1^3}{r_3^3}+\varepsilon_2\frac{r_2^3}{r_3^3}\right), \tag{8}$$

where the superscripts CdSe, CdS and ZnSe represent the core and the shells regions, respectively, $\varepsilon_{1(2)}$ are the relative mismatch defined as

$$\varepsilon_{1(2)}=\frac{a_{CdS(ZnSe)}-a_{CdSe(CdS)}}{a_{CdSe(CdS)}}, \tag{9}$$

being ν the Poisson ratio. The intraband absorption coefficient expression, given by S.L. Chuang [44], is:

$$\alpha(\hbar\omega)=\left(\frac{\pi\omega}{n_r c\epsilon_0}\right)\frac{2}{V}\sum_k|\vec{e}\cdot\vec{\mu}_{fi}|^2\delta(E_f-E_i-\hbar\omega), \tag{10}$$

Table 1
Used materials parameters [28,32].

	CdSe	CdS	ZnSe
m^*	0.15 m_e	0.22 m_e	0.21 m_e
a (nm)	0.605	0.582	0.565
ν	0.408	0.410	0.376
E_g^0 (eV)	1.74	2.49	2.69
a_v (eV)	0.9	0.4	1.65
a_c (eV)	−2	−2.54	−4.17
E_v^0 (eV)	−6.00	−6.42	−6.07

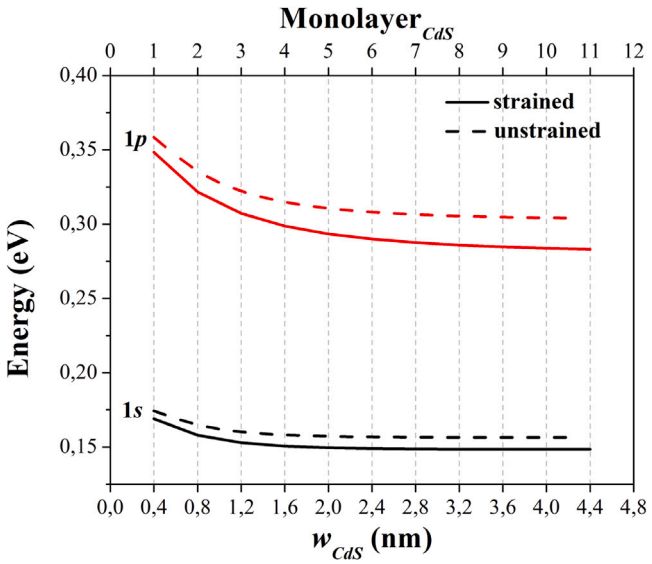

Fig. 2. $1s$- and $1p$-state energy levels as function of the CdS shell width (w_{CdS}) for strained (solid lines) and unstrained (dashed line) spherical *CdSe/CdS/ZnSe* CSS-QD. The core radius is r_{CdSe} = 2.8 nm and the ZnSe shell width is w_{ZnSe} = 0.66 nm.

here $\vec{\mu}_{fi} = \langle f|\vec{e}\cdot\vec{r}|i\rangle$ and the Dirac *delta* function can be represented as a Lorentzian function, as follows:

$$\delta(E_f - E_i - \hbar\omega) = \frac{\Gamma/2\pi}{(E_f - E_i - \hbar\omega)^2 - \left(\frac{\Gamma}{2}\right)^2}, \tag{11}$$

with Γ = 30 meV. The initial energy (E_i) and final one (E_f) corresponds to the $1s$- and $1p$-state, respectively, and $\hbar\omega$ stands for the incident photon energy. Here we use $\Delta m = 0$ and considered a linear z-polarization, so that,

$$\langle f|\vec{e}\cdot\vec{r}|i\rangle = \int \left\{Y_1^0(\theta,\varphi)R_{11}(r)\right\}^* r\cos\theta\, Y_0^0(\theta,\varphi) R_{00}(r)r^2\sin\theta\, dr d\theta d\varphi, \tag{12}$$

where Y_ℓ^m are the well known spherical harmonics [45].

3. Results and discussion

In this section, we present the computations of the strain effect in the electronic structure and intraband optical absorption coefficient for a spherical CSS-QD composed by a CdSe core, CdS inner shell and ZnSe outer shell, as represented in Fig. 1. The lattice mismatches values are $\varepsilon_1 = 0.038$ and $\varepsilon_2 = 0.029$. We used a core radius of 2.8 nm because the system begun to confine two states (the $1s$ and $1p$). Table 1 contains the material's parameters used in the calculations.

Fig. 2 shows the $1s$- and $1p$-state energy levels as function of the CdS shell width w_{CdS} from 0.4 to 4.4 nm (1–11 monolayers) for strained (solid lines) and unstrained (dashed lines) spherical core–shell–shell *CdSe/CdS/ZnSe* quantum dot. The CdSe core radius (r_{CdSe}) and ZnSe shell width (w_{ZnSe}) are fixed to 2.8 and 0.66 nm, respectively. We can

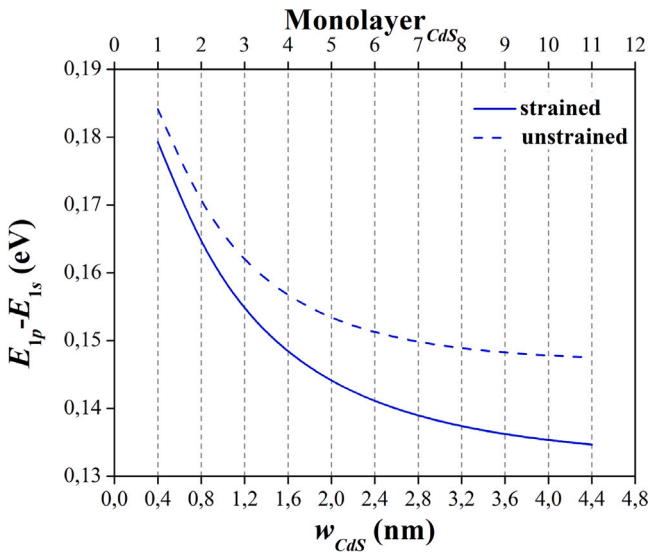

Fig. 3. Main energy difference between the $1s$- and $1p$-state energy levels as function of the CdS shell width (w_{CdS}). The CdSe core radius is r_{CdSe} = 2.8 nm while the ZnSe shell is w_{ZnSe} = 0.33 nm.

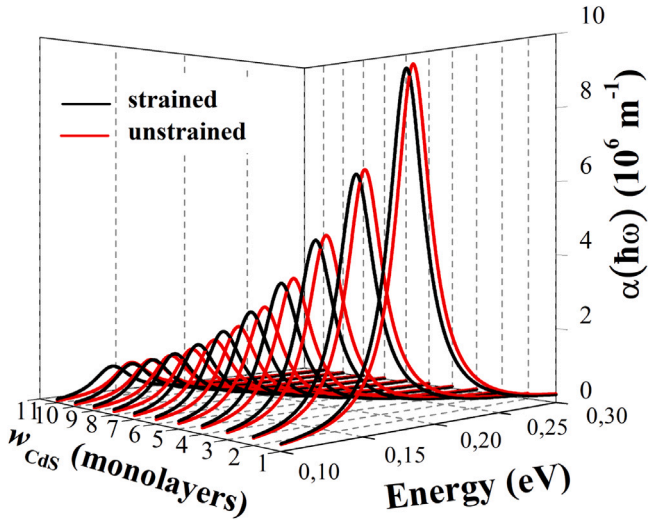

Fig. 4. Intraband absorption coefficient as function of the incident energy photon for spherical CdSe/CdS/ZnSe CSS-QD for w_{CdS} from 0.4 to 4.4 nm, with r_{CdSe} = 2.8 nm and w_{ZnSe} = 0.33 nm. The red and black line represents unstrained and strained quantum dot, respectively.

notice that the energy levels diminished as w_{CdS} increases, and the ground state ($1s$-state) is almost flat starting from w_{CdS} about 2.4 nm. The energy values of the strained system are lower than those that corresponds to the unstrained system.

In Fig. 3, the energy difference ($E_{1p} - E_{1s}$) between the $1s$- and $1p$-state, for strained and unstrained systems is presented. $E_{1p} - E_{1s}$ behavior is alike as that exhibit for each state in Fig. 2, but we must stress that the consideration of the strain effect give a lower energy difference in comparison with unstrained system. The strained and the unstrained CSS-QD energy difference range are 0.179–0.135 eV and 0.184–0.147 eV, respectively. We can see that the strain importantly affected the energy levels difference and consequently will be reflected in the intraband absorption coefficient peak location, as will be discussed below.

Intraband absorption coefficient as function of the incident-photon energy for the same configuration, as in Fig. 2, is presented in Fig. 4.

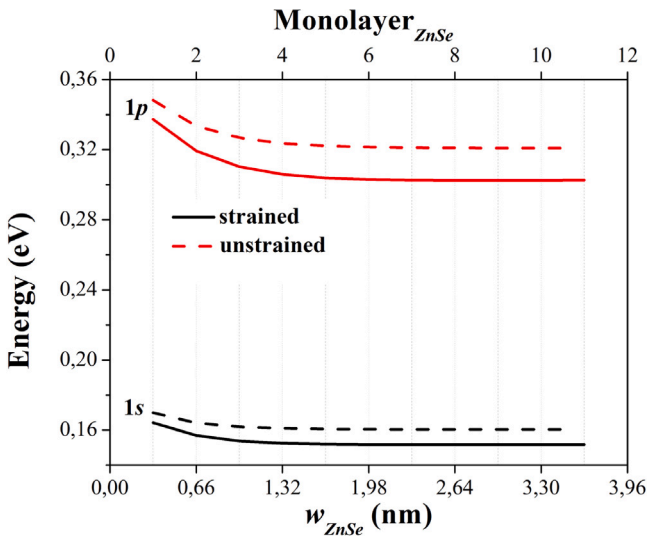

Fig. 5. $1s$- and $1p$-state energy levels as function of the outer shell size w_{ZnSe} for a strained (solid line) and unstrained (dashed line) spherical CdSe/CdS/ZnSe CSS-QD. The core radius is r_{CdSe} = 2.8 nm and the CdS inner shell is w_{CdS} = 0.8 nm.

Black and red lines represent the strained and unstrained CSS-QD configurations, respectively. By comparing the strained and the unstrained system, we can notice that the IAC resonant peak locates in lower energies (or has a redshift), the same situation occurs when the w_{CdS} increases, these results are consistent with the results in Fig. 3 computations, as predicted above. The intensity in the IAC decrease as w_{CdS} rises due to its dependence on $1/V$.

Fig. 5 reported the $1s$ (black lines) and $1p$ (red lines) energy levels as function of the outer shell size w_{ZnSe} (ranging within 1–3.63 nm or 1–11 monolayers) for a strained (solid lines) and unstrained (dashed lines) CdSe/CdS/ZnSe QD, with a core radius of r_{CdSe} = 2.8 nm and the CdS inner shell w_{CdS} = 0.8 nm. The behavior of the energy levels are alike to those shown as function of the inner shell width w_{CdS}. However, they are in different energy region, determined by the chosen parameters. But the most important fact is that the energy levels become unaffected (flat) for outer shell sizes (w_{ZnSe}) starting from 6 monolayers (about 1.98 nm) for the $1s$-state and from 7 monolayers (about 2.31 nm) for the $1s$-state, that means that the outer shell can modify the energy levels structure for values of w_{ZnSe} smaller than 2.5 nm, approximately. The energy difference between the $1s$- and $1p$-state is shown in Fig. 6, and as the w_{ZnSe} rises, the $E_{1p} - E_{1s}$ decreases.

Finally, in Fig. 7 we present the intraband absorption coefficient as a function of the incident photon energy for the spherical CdSe/CdS/ZnSe QD, w_{ZnSe} from 0.33 to 3.3 nm, with r_{CdSe} = 2.8 nm and w_{CdS} = 0.8 nm. The resonant peak of the IAC for the strained system exhibits a redshift respect to the unstrained system and as the w_{ZnSe} increases. The redshift can easily be understood with results of Fig. 6 because, as discussed above, the main energy difference is lower for strained than for unstrained system. In fact, the redshift for w_{ZnSe} = 0.33 nm is about 0.004 eV and as w_{ZnSe} increases it reaches almost 0.010 eV. Once again the diminishing in the magnitude of the intraband absorption coefficient obeys the $1/V$ dependency from Eq. (10), because as the outer shell width increases, the volume of the CSS-QD also augment.

4. Conclusions

In this work, we have investigated the electronic structure and the intraband absorption coefficient under the presence of the strain effect. The main conclusion of this work is that the strain effect represent a small but important factor in the calculated electronic and optical

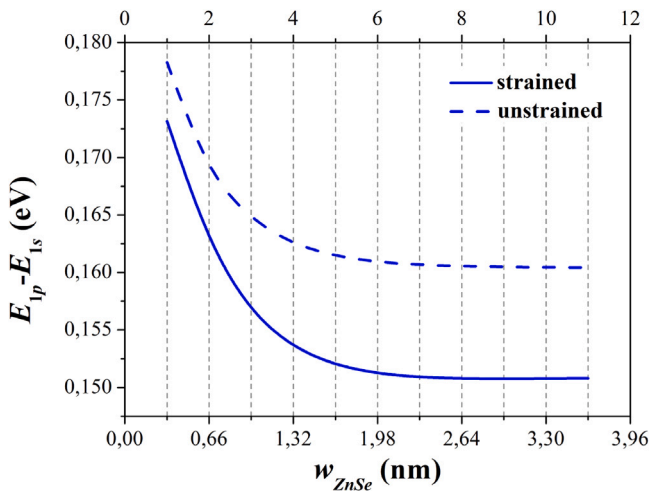

Fig. 6. Energy difference between the $1s$ and $1p$ energy levels as function of w_{ZnSe}. The core radius and the inner shell size is r_{CdSe} = 2.8 nm and w_{CdS} = 0.8 nm, respectively.

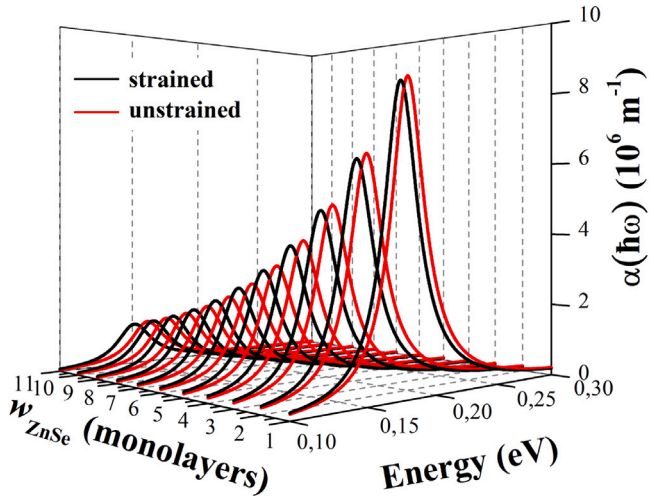

Fig. 7. Intraband absorption coefficient as function of the incident photon energy for spherical CdSe/CdS/ZnSe CSS-QD for when the outer shell size (w_{ZnSe}) increases from 0.33 to 3.3 nm. r_{CdSe} = 2.8 nm and w_{CdS} = 0.8 nm.

properties. The unstrained and strained system was compared and the results shown that the strain effect causes a redshift from 3% to 8% in the electronic states and in the IAC. As the inner and outer shell sizes augmented, the intraband absorption coefficient undergoes a redshift about 0.044 and 0.037 eV, respectively. The CdSe/CdS/ZnSe quantum dot exhibits a higher absorption range that of the CSS-QDs III–V counterpart. From the theoretical point of view, this methodology can be used to study other II–VI heterostructures, since it considers the deformation effect on spherical symmetries within the effective mass theory and the standard elasticity theory. In fact, the idea of theoretically comparing the study with and without deformation was to emphasize the importance of correctly characterizing the heterostructures that are naturally deformed, due to the difference in the lattice constant between materials. From the applied point of view, these studies help to design core/shell or core/shell/shell quantum dots by predicting the interband absorption coefficient of light, and varying the barrier widths and heights at will. These calculations can give experimenters information to synthesize quantum dots with desired properties.

CRediT authorship contribution statement

K.A. Rodríguez-Magdaleno: Conceptualization, Validation, Software, Methodology, Writing – original draft. **R. Pérez-Álvarez:** Methodology, Validation, Writing – review & editing. **F. Ungan:** Writing – review & editing, Validation, Methodology. **J.C. Martínez-Orozco:** Funding acquisition, Methodology, Project administration, Software, Validation.

Declaration of competing interest

The authors declare that they have no known competing financial interests or personal relationships that could have appeared to influence the work reported in this paper.

Acknowledgments

The authors acknowledge to CONACyT-SEP México for the financial support through grant number A1-S-8842 entitled "*Estudio de propiedades optoelectrónicas básicas en pozos, puntos y anillos cuánticos de materiales III–V y II–VI y sus heteroestructuras*". R. Pérez-Álvarez give thanks to the Autonomous University of Zacatecas, Mexico for the hospitality and to CONACyT-México for its financial support for the sabbatical stay.

References

[1] Prashant V. Kamat, Quantum dot solar cells. the next big thing in photovoltaics, J. Phys. Chem. Lett. 4 (6) (2013) 908–918.
[2] A.M. See, O. Klochan, A.P. Micolich, M. Aagesen, P.E. Lindelof, A.R. Hamilton, A study of transport suppression in an undoped AlGaAs/GaAs quantum dot single-electron transistor, J. Phys.-Condens. Matter 25 (2013) 505302.
[3] Sourav Adhikary, Subhananda Chakrabarti, Spectral broadening due to post-growth annealing of a long-wave InGaAs/GaAs quantum dot infrared photodetector with a quaternary barrier layer, Thin Solid Films 552 (2014) 146–149.
[4] M. Heidemann, S. Höfling, M. Kamp, (In,Ga)As/GaP electrical injection quantum dot laser, Appl. Phys. Lett. 104 (1) (2014) 011113.
[5] Young-Shin Park, Jeongkyun Roh, Benjamin T. Diroll, Richard D. Schaller, Victor I. Klimov, Colloidal quantum dot lasers, Nat. Rev. Mater. 6 (5) (2021) 382–401.
[6] A. John Peter, K. Navaneethakrishnan, Hydrogenic donor in a spherical quantum dot with different confinements, Chin. Phys. Lett. 26 (8) (2009) 087302.
[7] Mehmet Şahin, Koray Köksal, The linear optical properties of a multi-shell spherical quantum dot of a parabolic confinement for cases with and without a hydrogenic impurity, Semicond. Sci. Technol. 27 (12) (2012) 125011.
[8] Hatice Taş, Mehmet Şahin, The inter-sublevel optical properties of a spherical quantum dot-quantum well with and without a donor impurity, J. Appl. Phys. 112 (2012) 053717.
[9] Pekka Pietiläinen, Tapash Chakraborty, Energy levels and magneto-optical transitions in parabolic quantum dots with spin–orbit coupling, Phys. Rev. B 73 (2006) 155315.
[10] Najmeh Ehsanfard, Mohammad Reza Kazerani Vahdani, Intersubband optical absorption coefficients and refractive index changes in a Gaussian spherical quantum dot, Internat. J. Theoret. Phys. 54 (7) (2015) 2419–2435.
[11] A. Dehyar, G. Rezaei, A. Zamani, Electronic structure of a spherical quantum dot: Effects of the Kratzer potential, hydrogenic impurity, external electric and magnetic fields, Physica E 84 (2016) 175–181.
[12] Bekir Çakır, Yusuf Yakar, Ayhan Özmen, Linear and nonlinear absorption coefficients of spherical quantum dot inside external magnetic field, Phys. B 510 (2017) 86–91.
[13] W.H. Liu, Y. Qu, S.L. Ban, Intersubband optical absorption between multi energy levels of electrons in InGaN/GaN spherical core–shell quantum dots, Superlattices Microstruct. 102 (2017) 373–381.
[14] K.A. Rodríguez-Magdaleno, R. Pérez-Álvarez, J.C. Martínez-Orozco, R. Pernas-Salomón, Multi-shell spherical GaAs/$Ga_xAl_{1-x}As$ quantum dot shells-size distribution as a mechanism to generate intermediate band energy levels, Physica E 88 (2017) 142–148.
[15] D.A. Baghdasaryan, D.B. Hayrapetyan, V.A. Harutyunyan, Optical transitions in semiconductor nanospherical core/shell/shell heterostructure in the presence of radial electrostatic field, Phys. B 510 (2017) 33–37.
[16] D.B. Hayrapetyan, D.A. Baghdasaryan, E.M. Kazaryan, S.I. Pokutnyi, H.A. Sarkisyan, Exciton states and optical absorption in core/shell/shell spherical quantum dot, Chem. Phys. 506 (2018) 26–30.
[17] A. El Aouami, E. Feddi, A. Talbi, F. Dujardin, C.A. Duque, Electronic state and photoionization cross section of a single dopant in GaN/InGaN core/shell quantum dot under magnetic field and hydrostatic pressure, Appl. Phys. A 124 (2018) 442.
[18] K.A. Rodríguez-Magdaleno, R. Pérez-Álvarez, J.C. Martínez-Orozco, Intra-miniband absorption coefficient in GaAs/$Ga_xAl_{1-x}As$ core/shell spherical quantum dot, J. Alloys Compd. 736 (2018) 211–215.
[19] K.A. Rodríguez-Magdaleno, M.E. Mora-Ramos, R. Pérez-Álvarez, J.C. Martínez-Orozco, Effect of the hydrostatic pressure and shell's Al composition in the intraband absorption coefficient for core/shell spherical GaAs/$Ga_xAl_{1-x}As$ quantum dots, Mater. Sci. Semicond. Proc. 108 (2020) 104906.
[20] J.A. Osorio, D. Caicedo-Paredes, J.A. Vinasco, A.L. Morales, A. Radu, R.L. Restrepo, J.C. Martínez-Orozco, A. Tiutiunnyk, D. Laroze, Nguyen N. Hieu, Huynh V. Phuc, M.E. Mora-Ramos, C.A. Duque, Pyramidal core–shell quantum dot under applied electric and magnetic fields, Sci. Rep. 10 (2020) 8961.
[21] Bashir Mohi Ud Din Bhat, Rayees Ahmad Zargar, Effect of electric field and dot radius on the quantum state energies of an electron confined in a GaAs/$Ga_xAl_{1-x}As$ core shell quantum dot, Comput. Condens. Matter 12 (2017) 14–18.
[22] Dmitri V. Talapin, Ivo Mekis, Stephan Götzinger, Andreas Kornowski, Oliver Benson, Horst Weller, CdSe/CdS/ZnS and CdSe/ZnSe/ZnS core–shell–shell nanocrystals, J. Phys. Chem. B 108 (2004) 18826–18831.
[23] Yao He, Hao-Ting Lu, Li-Man Sai, Yuan-Yuan Su, Mei Hu, Chun-Hai Fan, Wei Huang, Lian-Hui Wang, Microwave synthesis of water-dispersed CdTe/CdS/ZnS core–shell–shell quantum dots with excellent photostability and biocompatibility, Adv. Mater. 20 (2008) 3416–3421.
[24] Xin Tong, Zhiming M. Wang, Quantum Dots Synthesis, Properties and Devices, Springer International Publishing, 2020.
[25] A.M. Smith, A.M. Mohs, S. Nie, Tuning the optical and electronic properties of colloidal nanocrystals by lattice strain, Nat. Nanotechnol. 4 (2009) 56–63.
[26] T.O. Cheche, V. Barna, I. Stamatin, Theoretical approach for type-i semiconductor spherical core–shell quantum dots heterostructure with wide band gaps, J. Optoelectron. Adv. Mater. 15 (2013) 615–620.
[27] T.O. Cheche, V. Barna, Y.-C. Chang, Analytical approach for type-II semiconductor spherical core–shell quantum dots heterostructures with wide band gaps, Superlattices Microstruct. 60 (2013) 475–486.
[28] Tudor E. Pahomi, Tiberius O. Cheche, Strain influence on optical absorption of giant semiconductor colloidal quantum dots, Chem. Phys. Lett. 612 (2014) 33–38.
[29] Deokho Jang, Younho Han, Seungin Baek, Jungho Kim, Theoretical comparison of the energies and wave functions of the electron and hole states between CdSe- and InP-based core/shell/shell quantum dots: effect of the bandgap energy of the core material on the emission spectrum, Opt. Mater. Express 9 (2019) 1257–1270.
[30] M.-W. Meng, L. Shi, Conversion efficiency of strained type-II core/shell quantum dot solar cell, Optoelectron. Lett. 15 (2019) 343–346.
[31] L. Shi, Z.-W. Yan, Conversion efficiency of strained core/shell quantum dot solar cell: Converting from type-I to type-II structures, J. Appl. Phys. 125 (2019) 174302.
[32] Chris G. Van de Walle, Band lineups and deformation potentials in the model-solid theory, Phys. Rev. B 39 (1989) 1871–1883.
[33] S. Pokrant, K.B. Whaley, Tight-binding studies of surface effects on electronic structure of CdSe nanocrystals: the role of organic ligands, surface reconstruction, and inorganic capping shells, Eur. Phys. J. D 6 (1999) 255–267.
[34] E.J. Tyrrell, J.M. Smith, Effective mass modeling of excitons in type-II quantum dot heterostructures, Phys. Rev. B 84 (2011) 165328.
[35] Nirmal Ganguli, S. Acharya, I. Dasgupta, First-principles study of the electronic structure of CdS/ZnSe coupled quantum dots, Phys. Rev. B 89 (2014) 245423.
[36] R. Kostić, D. Stojanović, Nonlinear optical spectra of intersubband transitions in a CdSe/ZnS/CdSe/SiO_2 spherical quantum dot, J. Nanosci. Nanotechnol. 12 (2012) 8528–8536.
[37] S.N. Saravanamoorthy, A. John Peter, Chang Woo Lee, Optical absorption coefficients in a CdSe/$Pb_{1-x}Cd_xSe$/CdSe spherical quantum dot quantum well nanostructure, Physica E 63 (2014) 337–342.
[38] K. Suseel Rahul, Nayana Devaraj, Rosmy K. Babu, Smitha Mathew, K. Salini, Vincet Mathew, Intraband absorption of D- center in CdSe/CdS/CdSe/CdS multilayer quantum dot, J. Phys. Chem. Solids 106 (2017) 99–104.
[39] A. Chafai, I. Essaoudi, A. Ainane, R. Ahuja, Linear and nonlinear optical properties of donors inside a CdSe/ZnTe core/shell nanodot: Role of size modulation, Results Phys. 14 (2019).
[40] R. Kostić, D. Stojanović, Intersubband transitions in spherical quantum dot quantum well nanoparticle, Opt. Quantum Electron. 52 (2020).

[41] Bahareh Alsadat Ebrahimipour, Hassan Ranjbar Askari, Ali Behjat Ramezani, Investigation of linear optical absorption coefficients in core–shell quantum dot (QD) luminescent solar concentrators (LSCs), Superlattices Microstruct. 97 (2016) 495.
[42] T.E. Pahomi, S.B. Stanciu, Analytical approach for strain field in core multi-shell quantum dots, J. Optoelectron. Adv. Mater. 16 (2014) 501–507.
[43] D.J. BenDaniel, C.B. Duke, Space-charge effects on electron tunneling, Phys. Rev. 152 (1966) 683–692.
[44] Shun Lien Chuang, Physics of Optoelectronic Devices, first ed., Wiley, 2005.
[45] Milton Abramowitz, Irene A. Stegun, Handbook of Mathematical Functions with Formulas, Graphs, and Mathematical Tables, Dover, New York, 1964, ninth dover printing, tenth gpo printing edition.